Design and Fabrication of 3-D-Printed High-Gain Broadband Fresnel Zone Lens Using Hybrid Groove-Perforation Method for Millimeter-Wave Applications

Shiyu Zhang [ID], Pai Liu, and William Whittow [ID], *Senior Member, IEEE*

Abstract—**This letter presents a novel hybrid design approach for the Fresnel zone lenses (FZL). The method combines the two conventional design approaches: grooved and perforated methods. Perforated lenses minimize the shadow blockage that grooved lenses suffer from, and therefore provide improved antenna gain. However, the fabrication of the low refractive index regions in the perforated lenses is challenging due to the limited manufacturing resolution, which means low refractive index dielectrics cannot be realized. The proposed hybrid FZL design utilizes the perforated method for the inner regions and applies the grooved method for the outer regions. This letter describes the equations used to optimize the design and gives the general design guidelines. A hybrid FZL antenna that operates at the center frequency of 33 GHz is presented. Measurement results show that the hybrid FZL improved the realized gain by up to 3.2 dB and the –3 dB gain bandwidth by up to 2 GHz when compared with the equivalent grooved FZL.**

Index Terms—**3-D printing, dielectric lenses, Fresnel zone lens millimeter-wave.**

I. INTRODUCTION

A LENS is a well-known collimation component that is widely used for antenna directivity enhancement [1]–[3], to mitigate limitations of path loss for long-range applications, or to shape spot beams. Fresnel zone lenses (FZL) are known for their thin profile, short focal length, and planar geometry when compared with the traditional convex lenses, which benefit compact lens antenna designs [4]–[6]. It has been attractive for consumer applications where the cost and the size of the antenna are design criteria as well as their electromagnetic performance.

There are two main methods to design a single-material FZL. The first one is called the "grooved" method, which replaces the curved convex lens surface with a series of concentric grooves. The grooves have different thicknesses, which realizes individual refracting surfaces to adjust the phases of the waves that pass through, and achieves an equal phase condition across

the lens surface [7], [8]. However, because of the thickness difference between contiguous grooves, the grooved Fresnel lens (GFL) suffers the shadow blockage effect, which decreases the gain when it is used for antenna applications [9], [10]. A compact GFL with $F/D < 0.5$ is prone to the shadow blockage effect [10]. The second method is known as the "perforated" design. A perforated Fresnel lens (PFL) has a planar profile and is composed of a series of concentric dielectric rings with the same thickness. Each dielectric ring has its own effective relative permittivity $\varepsilon_{\mathrm{reff}}$ to offer phase compensation of the waves that pass through, which also realizes the equal phase across the lens surface. The desired $\varepsilon_{\mathrm{reff}}$ are realized by perforating the dielectric rings with varying the volume fractions of holes [11]. Because of the planar profile of the PFL, the shadow blockage effect can be minimized and the gain of a PFL can be improved by ∼1 dB compared with an equivalent GFL [9]. Recently, the advanced additive manufacturing (AM) technique has been applied to perforated lens fabrication; the air/dielectric ratio can be significantly increased with a reduced tooling cost thanks to the AM process [12]–[15].

Although the PFL has a better electromagnetic performance than the GFL, it is more challenging to fabricate the perforations due to the required tight tolerance of tooling. Sometimes a limited air/dielectric ratio is applied to prevent the material from physically cracking. Moreover, the rings of the PFL are constructed by periodical unit cells, and the unit cell designs follow the effective medium theory to define the $\varepsilon_{\mathrm{reff}}$. In practice, since the minimum manufacturable feature is applied, the unit cell size has to be large enough to realize a low air/dielectric ratio for a low $\varepsilon_{\mathrm{reff}}$ value [15]. However, an FZL has a decreased zone width from the center to the outer of the lens [16], [17]. Therefore, towards the outer radius of the lens, the unit cell may become greater than the width of the zone that hosts the unit cell. In practice, this situation is common when a large zone number or a large radius is chosen in the lens design. When the unit cell is larger than the zone width, the $\varepsilon_{\mathrm{reff}}$ of the fabricated zone may not accurately agree with the designed value, which reduces the effective aperture and gain of the lens.

In this letter, a novel hybrid single-material FZL design is proposed to take advantage of both GFL and PFL designs. The hybrid design includes both grooved and perforated features: it replaces the PFL zones that have the unit cell greater than the zone width by using the grooved zones, so the lens aperture size is not compromised. In addition, the inner part of the lens is still fabricated using the perforated design so the shadow blockage
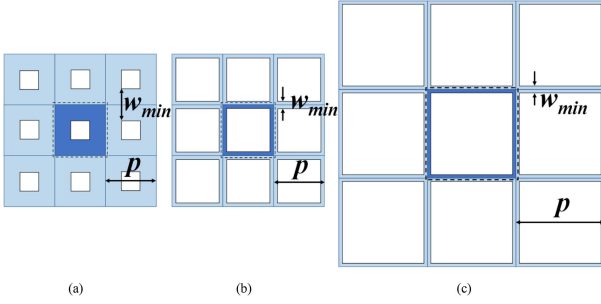
Fig. 1. Three unit cell designs. Dotted lines highlight one complete unit cell. The three unit cells have $\varepsilon_{\text{reff}(a)} > \varepsilon_{\text{reff}(b)} > \varepsilon_{\text{reff}(c)}$, $w_{\text{min}(a)} > w_{\text{min}(b)} = w_{\text{min}(c)}$, and $p_{(a)} = p_{(b)} < p_{(c)}$.
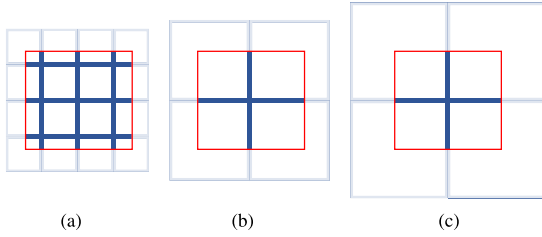

Fig. 2. Three perforated dielectrics that have designed effective permittivity $\varepsilon_{\text{reff}(a)} > \varepsilon_{\text{reff}(b)} > \varepsilon_{\text{reff}(c)}$. Red boxes highlight the limited spaces that can host the unit cells. Blue lines indicate the dielectrics and white areas are the air. Faded blue lines outside the red boxes are for visualizing the unit cell sizes and do not physically exist. In the limited spaces (outlined by the red boxes), the effective permittivities have $\varepsilon_{\text{reff}(a)} > \varepsilon_{\text{reff}(b)} = \varepsilon_{\text{reff}(c)}$.

Fig. 3. Hybrid FZL design sketch. (a) Fresnel zones and the cross section of a GFL. (b) PFL design. (c) Hybrid design.

can be minimized, which improves the gain and bandwidth of the lens compared with a GFL. To prove the concept, a hybrid FZL is presented. Three-dimensional (3-D) printing was used for rapid prototyping the lens and offers the capability of realizing an artificial dielectric with a high air/dielectric ratio and low $\varepsilon_{\text{reff}}$.

II. UNIT CELL AND HYBRID LENS DESIGN

A rectangular grid pattern was chosen to maximize the air/dielectric ratio, which enables a wide range of $\varepsilon_{\text{reff}}$ values to be realized. Fig. 1 shows the rectangular grid unit cell design. This heterogeneous unit cell is defined by the periodical dielectric grid lines. Air cubes are created by the surrounding dielectric grid lines. An effective way to reduce the $\varepsilon_{\text{reff}}$ of the unit cell is to reduce the grid line width so the air volume is increased, see Fig. 1(a) and (b). However, the line width cannot be reduced to an infinitesimal dimension in practice. And the minimum realizable line width is determined by the minimum manufacture feature size. In conventional perforation or injection molding manufacturing approaches, this can be the minimum distance between the perforated holes or the minimum width of the mold walls. Therefore, to further reduce the $\varepsilon_{\text{reff}}$ of the unit cell, the unit cell size (periodicity) can be increased but the dielectric line width remains the minimum manufacturable width, see Fig. 1(b) and (c). Note, the unit cell size should be smaller than the wavelength to satisfy the periodical boundary condition.

When the unit cells are used in a limited area, such as concentrical lens rings, extra care should be taken to ensure at least one complete unit cell falls in the defined space so the $\varepsilon_{\text{reff}}$ for that area is accurate. Fig. 2(a) shows a perforated dielectric material that has the unit cell smaller than the entire effective medium
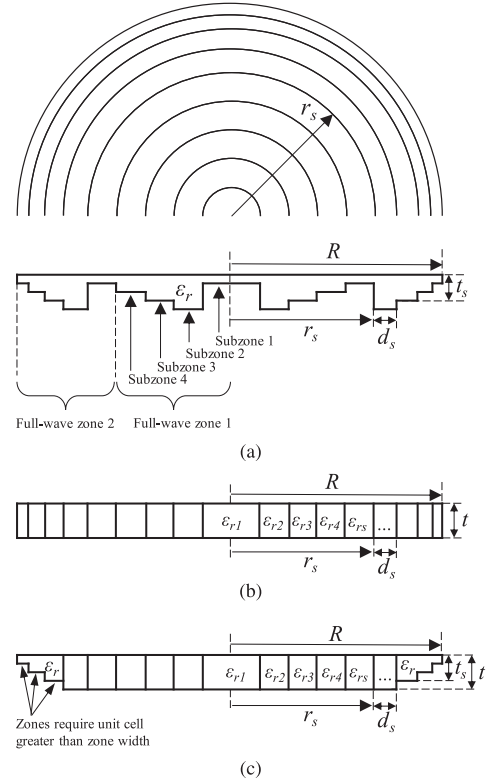
area; in this scenario, the $\varepsilon_{\text{reff}}$ is defined by the air/dielectric ratio of the unit cell. However, when the perforation unit cell is larger than the entire effective medium area, shown in Fig. 2(b) and (c), the calculated $\varepsilon_{\text{reff}}$ by using the effective medium theory is no longer accurate because Fig. 2(b) and (c) shows that the two dielectric areas have a similar air/dielectric ratio but the designed $\varepsilon_{\text{reff}(b)}$ in Fig. 2(b) is greater than $\varepsilon_{\text{reff}(c)}$, see Fig. 2(c). This inaccurate $\varepsilon_{\text{reff}}$ scenario often occurs at the outer region of the lens where the zone width is too small to host an entire unit cell.

The concept of the hybrid design, shown in Fig. 3, is to keep the perforated inner part that has the unit cell smaller than the zone width and use the grooved design for the outer part that has the unit cell larger than the zone width. An FZL has multiple full-wave zones and subzones, shown in Fig. 3(a). The equivalent GFL in Fig. 3(a) and PFL in Fig. 3(b) have the same radius, the number of subzones and the subzones widths. The hybrid FZL in Fig. 3(c) utilizes the perforated dielectrics that have the same thickness in the central part of the lens. For the outer region of the hybrid lens, the grooved dielectric zones that have the same dielectric constant are applied.

In an FZL, a subzone is a part of one full-wave zone. The wave that passes through all the full-wave zones will be considered to have the same phase. The full-wave zone is usually divided into P subzones and each subzone will correct the phase every $2\pi/P$. Usually, the subzone number P is chosen as 4, 8, or 16 that means each subzone will correct the phase every π/P. A large P value leads to a small phase difference between adjacent subzones for maximum radiation efficiency of the FZL; and to a narrow subzone width, which requires smaller unit cells to be completely fitted in the zone. This requires a fine manufacture feature size with tight tolerance.

The full-wave zone number W can be estimated by

$$W = \frac{\sqrt{F^2 + R^2} - F}{\lambda} \qquad (1)$$

where R is the radius of the lens, F is the focal length, and λ is the design wavelength. The focal length and the lens diameter result in the full-wave zone number $W = 3$.

The outer radius of sth subzone of the FZL is obtained by [7]

$$r_s = \sqrt{\frac{2s\lambda F}{P} + \left(\frac{s\lambda}{P}\right)^2}, \quad s = 1, 2, \ldots, WP \qquad (2)$$

where s is the subzone number, and WP is the product of W and P. The zone number s determines the location of this subzone.

The subzone width of sth subzone d_s is

$$d_s = r_s - r_{s-1}, \ s = 1, 2, \ldots, WP, \ r_0 = 0 \qquad (3)$$

The required ε_r of each subzone can be found by:

$$\varepsilon_{rs} = \left\{ \frac{\sqrt{\varepsilon_{rmax}} - \sqrt{\varepsilon_{r0}}}{P - 1} \left[(WP - s + 1) \mod P\right] + \sqrt{\varepsilon_{r0}} \right\}^2$$
$$s = 1, 2, \ldots, WP \qquad (4)$$

where $\mod$ is the modulo operation to find the remainder after a division, ε_{rmax} is the maximum material relative permittivity equal to the permittivity of the 3-D-print filament, and $\varepsilon_{r0} = 1$.

Then, unit cell simulations with periodic boundary conditions were carried out to determine the perforation unit cell structures for the desired ε_r values. The unit cell size can be estimated from the material infill % [18]

$$i = \frac{\varepsilon_r - \varepsilon_{r0}}{\varepsilon_{rmax} - \varepsilon_{r0}} \qquad (5)$$

The unit cell size (periodicity) p is a function of the infill percentage i and the minimum infill grid width w_{min}

$$p = \frac{w_{min} + w_{min}\sqrt{1 - i}}{i} \qquad (6)$$

Once the unit cell is finalized, the unit cell size is used to compare with the subzone width d_s to decide whether a grooved subzone should be used. The thicknesses of the grooved zones depend on their location of the subzone and are different from each other, which can be found by

$$t_{gs} = \frac{\lambda}{\left(\sqrt{\varepsilon_r} - \sqrt{\varepsilon_{r0}}\right) P} \left[(WP - s + 1) \mod P\right]$$
$$s = 1, 2, \ldots, WP. \qquad (7)$$

The thicknesses of all perforated subzones t_p are the same

$$t_p = \frac{\lambda}{\left(\sqrt{\varepsilon_r} - \sqrt{\varepsilon_{r0}}\right) P} (P - 1). \qquad (8)$$

III. RESULTS

In this letter, the lens is designed to operate at the center frequency of 33 GHz. The lens is fed by an WR28 open-ended waveguide. The edge taper is chosen at −10 dB, which is considered as the optimal value for dielectric lens antennas [19]. The lens is designed to have a focal length of 30 mm and a diameter of ~100 mm, which results in an F/D ratio of ~ 0.3.

TABLE I
LENS PARAMETERS AS CALCULATED FROM (1) TO (8) FOR THE GROOVED LENS (GFL), PERFORATED LENS (PFL), AND HYBRID LENS (HL)

Subzone number		1	2	3	4	5	6	7	8	9	10	11	12
Radius / mm		11.9	17.1	21.3	25.1	28.5	31.7	34.8	37.7	40.6	43.4	46.1	48.8
Thickness / mm	GFL	0	9.3	6.2	3.1	0	9.3	6.2	3.1	0	9.3	6.2	3.1
	PFL	9.3											
	HL	9.3							3.1	0	9.3	6.2	3.1
Relative Permittivity	GFL	3											
	PFL	1	3	2.2	1.5	1	3	2.2	1.5	1	3	2.2	1.5
	HL	1	3	2.2	1.5	1	3	2.2	3				

The lens was 3-D printed by using the low-cost fused filament fabrication 3-D-printer (Raise 3-D) with low-loss ABS based 3-D-print filament PREPERM TP20279 ($\varepsilon_r = 3$, $tan\delta = 0.0046$). The infilled grid lines were extruded by the printer nozzle that has a 0.4 mm diameter. The nozzle diameter determines the size of the minimum printed feature. The relationship between the unit cell size and the ε_{reff} was simulated by using CST Studio Suite. The unit cell size for $\varepsilon_{reff} = 2.2$ is 1.1 mm, and for $\varepsilon_{reff} = 1.5$ is 3 mm. Simulations of the unit cell designs showed stable angular stability, which ensured the effective permittivity remains constant when the incident angles (in both axes) were increased up to 60°.

The lenses with $P = 2$, 4, 6, and 8 were simulated. The lens with $P = 2$ had a relatively low gain and bandwidth when comparing with the lenses with $P = 4$, 6, and 8. However, the lenses with $P = 6$ and 8 had narrow subzone widths, which means that the required unit cells cannot be realized using the 0.4 mm 3D printer nozzle. Therefore, $P = 4$ was chosen.

The final designed parameters of the hybrid FZL are shown in Table I. The parameters of the equivalent GFL and PFL are also included for comparison. The lowest permittivity is made to equal to 1 so air rings can be used to minimize the weight. The design sketch of the proposed hybrid lens is shown in Fig. 4. The zones that have $\varepsilon_r < 3$ were realized by the perforated dielectrics with grid infill patterns.

For comparison, a GFL was also fabricated. Note, the PFL cannot be fabricated as the unit cells at the outer region of the lens were larger than the subzone width. Therefore, only the simulated results of the PFL were included for comparison. CST Studio Suite was used for the full-wave simulations. The effective dielectric mediums with the grid infill patterns were simulated as homogeneous dielectrics for reducing the required computational resources. Therefore, the simulated PFL was an ideal case and the simulated results of the PFL were used to benchmark the lenses' performance. The feed points of all three lenses were optimized so the highest directivities were obtained at the design frequency of 33 GHz. Note, the optimized feed distance of the GFL is ~1 mm longer than the feed distances of the hybrid FZL and PFL. The hybrid FZL and the GFL were measured in a spherical near-field anechoic chamber. The fabricated hybrid FZL and the GFL are shown in Fig. 5(a) and the measurement setup is shown in Fig. 5(b).

The measured directivity patterns at the frequencies of 30, 32, 34, and 36 GHz show good agreement with the simulations see Fig. 6. The measured side lobes were all under −16 dB, and the 3 dB beamwidth ranged from 5.1° to 6.8°. The directivity as a function of the frequency of the hybrid FZL and the GFL are
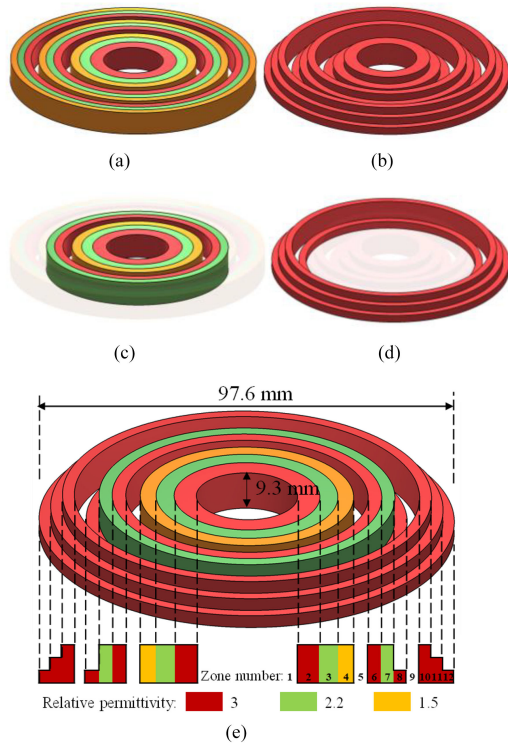
Fig. 4. Design sketch of the proposed hybrid FZL. (a) PFL. (b) GFL. (c) Perforated part of the PFL that is used for the hybrid FZL. (d) Grooved part of the GFL that is used for the hybrid FZL. (e) Hybrid FZL that has the perforated center and the grooved outer. Each color represented different ε_r.
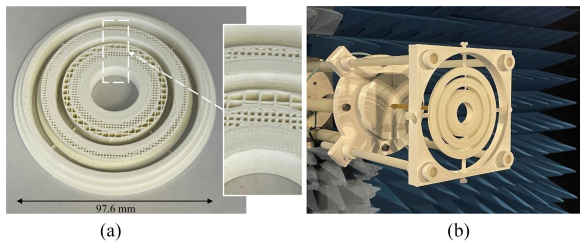

Fig. 5. (a) Photographs of the fabricated hybrid lens, with zoomed-in view of perforated zones that utilize the rectangular grid patterns. (b) Measurement setup: the lens holder was 3-D-printed and hollow to minimize the effect on the radiation pattern.
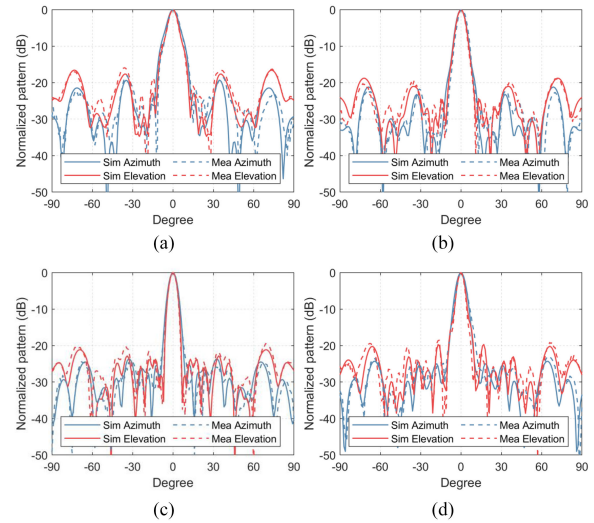

Fig. 6. Simulated and measured directivity patterns of the proposed hybrid FZL. (a) 30 GHz. (b) 32 GHz. (c) 34 GHz. (d) 36 GHz.
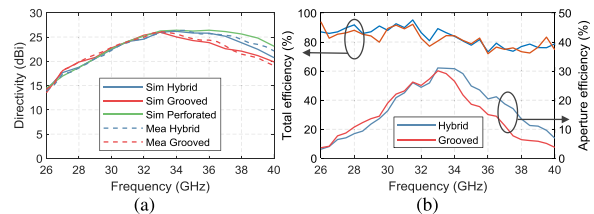

Fig. 7. (a) Simulated and measured directivity (left) of the hybrid FZL, and the equivalent GFL and PFL. (b) Measured total efficiency and the aperture efficiency (right) of the hybrid FZL and the GFL as a function of frequency.

$\sim$25%. The measured total efficiency and the aperture efficiency (both include the mismatch loss) of the hybrid FZL and the GFL are shown in Fig. 7(b). It shows that the proposed hybrid FZL antenna offers $\sim$74% to 95% total efficiency at the frequency range between 26 and 40 GHz with the aperture efficiency of up to 31.1% at the center frequency of 33 GHz, and the hybrid FZL clearly improves the aperture efficiency and the bandwidth compared with the GFL.

IV. CONCLUSION

In this letter, a high-gain and wideband FZL that utilized the groove-perforation hybrid method is proposed, additively manufactured, and verified experimentally. The hybrid approach has been developed to overcome the challenge when the perforated unit cell is larger than the Fresnel zone ring width. In practice, a tabular database for the manufacturable unit cell sizes and the $\varepsilon_{\text{reff}}$ can be created using (5) and (6). A perforated FZL can be initially designed based on the required *F/D* ratio. Then, the grooved rings are used to replace the perforated rings that have their width smaller than the required unit cell size. Compared with a GFL, the hybrid approach improves the directivity, total efficiency, aperture efficiency, and bandwidth of the lens antenna and offers the performance close to an ideal PFL which cannot be practically manufactured. The hybrid approach gives an extra degree of freedom for the design and fabrication of the FZL because the outer zones do not have to comprise the unit cell size of the effective dielectrics. This is particularly useful for the compact, low-cost mm-Wave lens antenna applications.

shown in Fig. 7(a), compared with the simulated directivity of the PFL. As shown in Fig. 7(a), the hybrid FZL offers a broadband performance that is close to an ideal PFL that is composed of multiple homogenous dielectric rings. Fig. 7(a) shows that hybrid FZL and GFL lenses have similar directivities below 33 GHz, which indicates that the diffraction due to the shadow blockage is small when the frequency is lower than the designed frequency of the lenses. However, the hybrid FZL improves the directivity by up to 3.2 dB at the higher-end frequencies when compared with the GFL. A hybrid FZL with a reduced number of outer grooved rings was also simulated, to verify the contribution of the outer grooved rings to the collimation of the main beam. After removing the five outer grooved rings, only the perforated region of the hybrid FZL is left, and the directivity of this smaller lens is $\sim$2.5 dB smaller than the full hybrid lens at the design frequency of 33 GHz. The measured realized gain (including the mismatch loss) of the hybrid FZL ranged from 13.2 dBi to 25.6 dBi, and achieved a −3 dB gain fractional bandwidth of

REFERENCES

[1] H. F. Ma, B. G. Cai, T. X. Zhang, Y. Yang, W. X. Jiang, and T. J. Cui, "Three-dimensional gradient-index materials and their applications in microwave lens antennas," *IEEE Trans. Antennas Propag.*, vol. 61, no. 5, pp. 2561–2569, May 2013.

[2] Z. Yang *et al.*, "Ultrawideband antipodal tapered slot antenna with gradient refractive index metamaterial lens," *IEEE Antennas Wireless Propag. Lett.*, vol. 18, no. 12, pp. 2741–2745, Dec. 2019.

[3] Y.-X. Zhang, Y.-C. Jiao, and S.-B. Liu, "3D-printed comb-mushroom-like dielectric lens for stable gain enhancement of printed log-periodic dipole array," *IEEE Antennas Wireless Propag. Lett.*, vol. 17, no. 11, pp. 2099–2103, Nov. 2018.

[4] H. D. Hristov and M. H. A. J. Herben, "Millimeter-wave Fresnel-zone plate lens and antenna," *IEEE Trans. Microw. Theory Techn.*, vol. 43, no. 12, pp. 2779–2785, Dec. 1995.

[5] L. P. Kamburov, J. M. Rodriguez, J. R. Urumov, and H. D. Hristov, "Millimeter-wave conical fresnel zone lens of flat dielectric rings," *IEEE Trans. Antennas Propag.*, vol. 62, no. 4, pp. 2140–2148, Apr. 2014.

[6] J. Xu, Z. N. Chen, and X. Qing, "270-GHz LTCC-integrated high gain cavity-backed Fresnel zone plate lens antenna," *IEEE Trans. Antennas Propag.*, vol. 61, no. 4, pp. 1679–1687, Apr. 2013.

[7] H. D. Hristov and J. M. Rodriguez, "Design equation for multidielectric Fresnel zone plate lens," *IEEE Microw. Wireless Compon. Lett.*, vol. 22, no. 11, pp. 574–576, Nov. 2012.

[8] B. Philips and A. D. Olver, "Design and performance of profiled dielectric loaded horns," *Proc. IEE Microw., Antennas Propag.*, vol. 141, no. 5, 1994, Art. no. 337.

[9] A. Petosa, A. Ittipiboon, and S. Thirakoune, "Shadow blockage improvement using a perforated dielectric Fresnel lens," in *Proc. IEEE Antennas Propag. Soc. Int. Symp.*, 2003, vol. 4, no. 2, pp. 514–517.

[10] A. Petosa and A. Ittipiboon, "Shadow blockage effects on the aperture efficiency of dielectric Fresnel lenses," *Proc. IEE Microw. Antennas Propag.*, vol. 147, no. 6, pp. 451–454, 2000.

[11] A. Petosa and A. Ittipiboon, "Design and performance of a perforated dielectric Fresnel lens," *Proc. IEE Microw. Antennas Propag.*, vol. 150, no. 5, 2003, Art. no. 309.

[12] S. Zhang, "Design and fabrication of 3D-printed planar Fresnel zone plate lens," *Electron. Lett.*, vol. 52, no. 10, pp. 833–835, May 2016.

[13] J. M. Monkevich and G. P. Le Sage, "Design and fabrication of a custom-dielectric Fresnel multi-zone plate lens antenna using additive manufacturing techniques," *IEEE Access*, vol. 7, pp. 61452–61460, 2019.

[14] G.-B. Wu, Y.-S. Zeng, K. F. Chan, S.-W. Qu, and C. H. Chan, "3-D printed circularly polarized modified Fresnel lens operating at terahertz frequencies," *IEEE Trans. Antennas Propag.*, vol. 67, no. 7, pp. 4429–4437, Jul. 2019.

[15] S. Zhang, R. K. Arya, W. G. Whittow, D. Cadman, R. Mittra, and J. Vardaxoglou, "Ultra-wideband flat metamaterial GRIN lenses assisted with additive manufacturing technique," *IEEE Trans. Antennas Propag.*, vol. 69, no. 7, pp. 3788–3799, Jul. 2020.

[16] H. D. Hristov and M. H. A. J. Herben, "Millimeter-wave Fresnel-zone plate lens and antenna," *IEEE Trans. Microw. Theory Techn.*, vol. 43, no. 12, pp. 2779–2785, Dec. 1995.

[17] D. N. Black and J. C. Wiltse, "Millimeter-wave characteristics of phase-correcting Fresnel zone plates," *IEEE Trans. Microw. Theory Techn.*, vol. 35, no. 12, pp. 1122–1129, Dec. 1987.

[18] S. Zhang, R. K. Arya, S. Pandey, Y. Vardaxoglou, W. Whittow, and R. Mittra, "3D-printed planar graded index lenses," *Microw., Antennas Propag.*, vol. 10, no. 13, pp. 1411–1419, Oct. 2016.

[19] A. V. Boriskin, R. Sauleau, and A. I. Nosich, "Performance of hemielliptic dielectric lens antennas with optimal edge illumination," *IEEE Trans. Antennas Propag.*, vol. 57, no. 7, pp. 2193–2198, Jul. 2009.